Review Article | Pediatric Imaging

eISSN 2005-8330
https://doi.org/10.3348/kjr.2020.1332
Korean J Radiol 2021;22(8):1397-1415

Korean Journal of Radiology
KJR

Pediatric Cardiothoracic CT Guideline Provided by the Asian Society of Cardiovascular Imaging Congenital Heart Disease Study Group: Part 2. Contemporary Clinical Applications

Hyun Woo Goo[1], Suvipaporn Siripornpitak[2], Shyh-Jye Chen[3], Oktavia Lilyasari[4], Yu-Min Zhong[5], Haifa Abdul Latiff[6], Eriko Maeda[7], Young Jin Kim[8], I-Chen Tsai[9], Dong Man Seo[10]

[1]Department of Radiology and Research Institute of Radiology, Asan Medical Center, University of Ulsan College of Medicine, Seoul, Korea; [2]Department of Diagnostic and Therapeutic Radiology, Faculty of Medicine, Ramathibodi Hospital, Mahidol University, Bangkok, Thailand; [3]Department of Medical Imaging, National Taiwan University, Medical College and Hospital, Taipei, Taiwan; [4]Department of Cardiology and Vascular Medicine, Universitas Indonesia, National Cardiovascular Center Harapan Kita, Jakarta, Indonesia; [5]Diagnostic Imaging Center, Shanghai Children's Medical Center, Shanghai, China; [6]Pediatric and Congenital Heart Centre, Institut Jantung Negara, Kuala Lumpur, Malaysia; [7]Department of Radiology, The University of Tokyo, Tokyo, Japan; [8]Department of Radiology, Severance Hospital, Yonsei University College of Medicine, Seoul, Korea; [9]Congenital Heart Disease Study Group Member of the Asian Society of Cardiovascular Imaging, Taichung, Taiwan; [10]Department of Cardiothoracic Surgery, Ewha Womans University Seoul Hospital, Seoul, Korea

The use of pediatric cardiothoracic CT for congenital heart disease (CHD) was traditionally limited to the morphologic evaluation of the extracardiac thoracic vessels, lungs, and airways. Currently, the applications of CT have increased, owing to technological advancements in hardware and software as well as several dose-reduction measures. In the previously published part 1 of the guideline by the Asian Society of Cardiovascular Imaging Congenital Heart Disease Study Group, we reviewed the prerequisite technical knowledge for clinical applications in a user-friendly and vendor-specific manner. Herein, we present the second part of our guideline on contemporary clinical applications of pediatric cardiothoracic CT for CHD based on the consensus of experts from the Asian Society of Cardiovascular Imaging CHD Study Group. This guideline describes up-to-date clinical applications effectively in a systematic fashion.

Keywords: *Cardiothoracic CT; Child; Congenital heart disease; Guideline*

INTRODUCTION

With its increased utility, cardiothoracic CT has replaced diagnostic catheter angiography in patients with congenital heart disease (CHD) [1,2]. CT protocols need to be optimized to prevent outliers with high radiation exposure [3] and, thus, to increase its benefit-risk ratio [4-6]. In patients with CHD, the clinical applications of CT have been traditionally confined to the morphologic evaluation of the extracardiac thoracic vessels, lungs, and airways [7,8]. The recent introduction of electrocardiography (ECG)-synchronized CT scan enables us to perform quantitative and functional evaluations of the cardiovascular structures [9,10]. In CHD, combined multiple cardiac defects are commoner than isolated ones and often associated with anomalies of other systems or organs. In such cases, a systematic organ-based approach seems to more appropriately demonstrate clinical applications compared to overlapped descriptions among specific cardiac defects as in the so-called systematic segmental approach commonly used to evaluate patients with CHD.

An expert consensus describing the rationale and utility

Received: November 9, 2020 **Revised:** January 27, 2021
Accepted: January 31, 2021
Corresponding author: Hyun Woo Goo, MD, PhD, Department of Radiology and Research Institute of Radiology, Asan Medical Center, University of Ulsan College of Medicine, 88 Olympic-ro 43-gil, Songpa-gu, Seoul 05505, Korea.
• E-mail: ghw68@hanmail.net

of CT in patients with CHD was previously provided by the Society of Cardiovascular Computed Tomography [11]. However, ample accounts on the clinical experiences with pediatric cardiothoracic CT in Asian countries [12] may provide more useful information about the practical applications. Furthermore, guidelines need to be updated to include new information. Therefore, we comprehensively discuss the contemporary organ-based clinical applications of pediatric cardiothoracic CT, as the second part of the guidelines provided by the Asian Society of Cardiovascular Imaging Congenital Heart Disease Study Group.

Pulmonary Artery

Most pulmonary artery anomalies are associated with CHD, and they may have underlying syndromes [13,14]. Cardiothoracic CT is useful for evaluating these pulmonary artery anomalies associated with CHD [11].

In tetralogy of Fallot, the most common congenital cyanotic heart disease, a broad spectrum of pulmonary artery hypoplasia in addition to pulmonary annular and infundibular narrowing is observed on CT [15]. The sizes of these structures are usually close to normal in pink tetralogy of Fallot. In contrast, pulmonary artery hypoplasia tends to be severer in patients with severe cyanosis, and severe infundibular narrowing is observed during hypoxic spells. This information is crucial for planning right surgical ventricular outflow tract reconstruction. In patients with severe pulmonary artery hypoplasia, a palliative shunt may be necessary to increase pulmonary artery flow.

In CHD, pulmonary artery stenosis may involve central or peripheral branches. Central stenosis occurs commonly in a juxtaductal region of the pulmonary artery, most commonly involving the left side. In contrast, peripheral stenosis is often associated with genetic syndromes, such as Williams and Alagille syndromes, and its morphologic types on CT varies from focal narrowing to long-segment hypoplasia. Recently, CT was used to provide an accurate quantitative measure of differential pulmonary vascularity in patients with pulmonary artery stenosis [16].

In pulmonary atresia and ventricular septal defect, multiple pulmonary arterial flow sources originate from the systemic arterial system, including a patent ductus arteriosus (PDA) or major aortopulmonary collateral arteries. CT is useful to accurately map the morphological characteristics, including the size, number, location, and stenosis, of these collateral arteries and small central pulmonary arteries at various stages of unifocalization (Fig. 1A) [17]. The presence and confluence of the central pulmonary artery can be evaluated accurately with CT although the size is small because of its high spatial and contrast resolutions [18]. The presence/absence of communication between the central pulmonary artery and the systemic arterial collaterals is also important for optimal surgical planning, which should be evaluated with CT (Fig. 1B) and subsequently confirmed on catheter angiography. Stenosis may be observed in the origin or proximal portion of the major aortic collaterals (Fig. 1C), and its presence decreases hemodynamic contribution of the affected collateral artery to total pulmonary arterial flow. The key role of CT is to reduce procedure time and

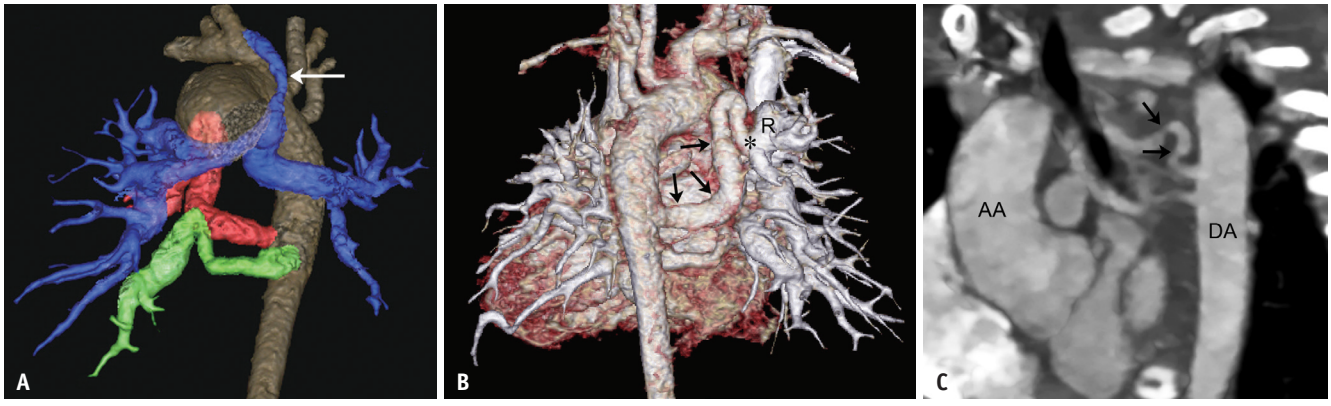

Fig. 1. Pulmonary atresia, ventricular septal defect, and major aortopulmonary collateral arteries.
A. Merged frontal volume-rendered CT image obtained in a 9-month-old girl illustrates color-coded pulmonary artery mapping including two major collateral arteries (red and greed) originating from the DA and the central pulmonary arteries (blue) supplied by a 4-mm central shunt (arrow). **B.** Posterior volume-rendered CT image obtained in a 6-month-old boy shows a connection (asterisk) between a larger aortopulmonary collateral artery (arrows) and the right central pulmonary artery (R). The pulmonary arteries appear dilated and tortuous, suggesting increased pulmonary arterial pressure. **C.** Oblique coronal reformatted CT image obtained in a 6-day-old boy shows two focal stenoses (arrows) at the proximal portion of one major aortopulmonary collateral artery. AA = ascending aorta, DA = descending aorta

https://doi.org/10.3348/kjr.2020.1332

Korean Journal of Radiology
KJR

potential diagnostic errors of preoperative diagnostic cardiac catheterization and help optimally plan unifocalization surgery.

In truncus arteriosus, a single great artery with a single semilunar valve supplies the pulmonary, systemic, and coronary circulations. Four types based on the branching pattern of the pulmonary artery can be accurately evaluated with CT, which is helpful for surgical planning (Fig. 2) [19].

Aortopulmonary window is a rare anomaly, characterized by abnormal communication between the ascending aorta and pulmonary artery and classified into the proximal, distal, and total defects depending on the location and extent of the defect (Fig. 3) [20].

In absent pulmonary valve syndrome, CT is useful for assessing vascular bronchial compressions due to markedly dilated pulmonary arteries before and after surgical treatment (Fig. 4) [21].

In left pulmonary artery sling, stenosis of the affected pulmonary artery and associated tracheobronchial abnormalities can be accurately evaluated with CT (Fig. 5) [22]. CT is also useful after reimplantation of the left pulmonary artery with or without tracheoplasty.

Pulmonary Vein

In anomalous pulmonary venous returns, where part or all of the pulmonary veins drain anomalously into the right atrium directly or indirectly, CT shows high diagnostic accuracy in delineating pulmonary vein morphology, obstruction of the pulmonary venous drainage, and associated anomalies [23,24].

Partial anomalous pulmonary venous return (PAPVR) involving at least one, but not all, pulmonary veins (Fig. 6) is usually asymptomatic or mildly symptomatic, and it is often detected incidentally. The anomaly most commonly involves the right upper thorax, in which the right upper pulmonary vein anomalously drains into the right atrium or the superior

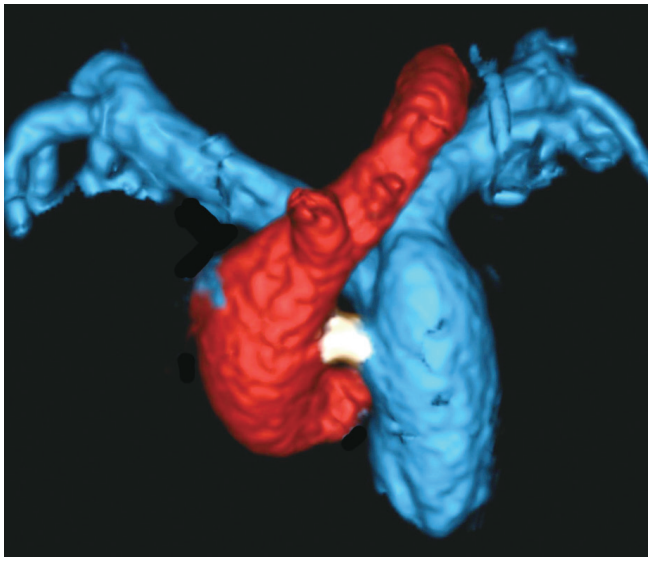

Fig. 3. Aortopulmonary window in a 1-month-old boy. Color-coded volume-rendered CT image with superior view demonstrates a small communication (white) between the ascending aorta (red) and the pulmonary trunk (blue) at their distal portion.

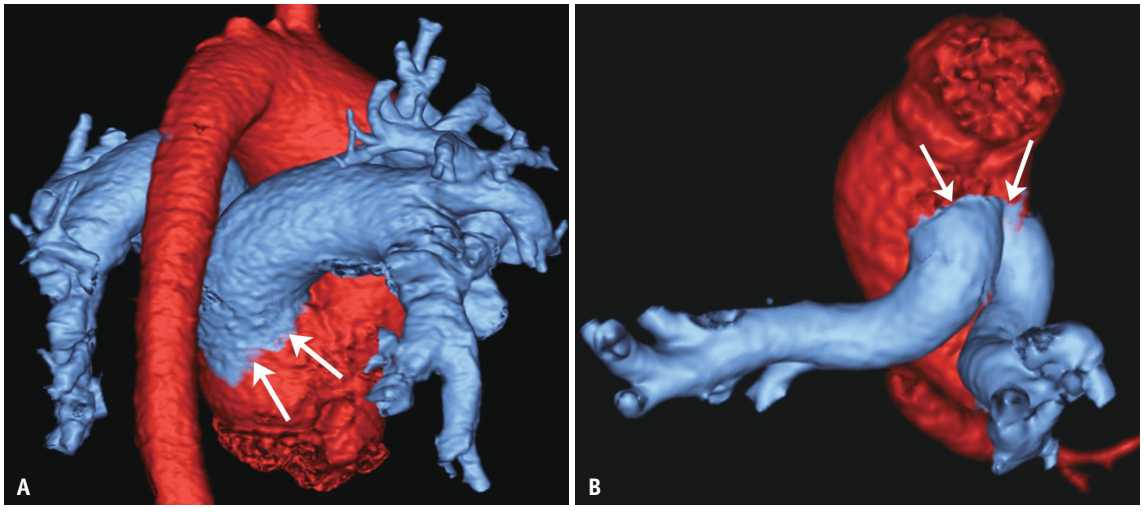

Fig. 2. Truncus arteriosus demonstrated on cardiothoracic CT.
A. In an 11-year-old girl, color-coded volume-rendered CT image with oblique posterior view shows truncus arteriosus type 1, in which the pulmonary trunk (blue) arises from the left lateral aspect (arrows) of the common arterial trunk (red) and divides into the right and left pulmonary arteries (blue). **B.** In a 1-year-old girl, color-coded volume-rendered CT image with inferior view demonstrates truncus arteriosus type 2, in which the right and left pulmonary arteries (blue) originate separately but close together directly from the posterior aspect (arrows) of the common arterial trunk (red).

https://doi.org/10.3348/kjr.2020.1332

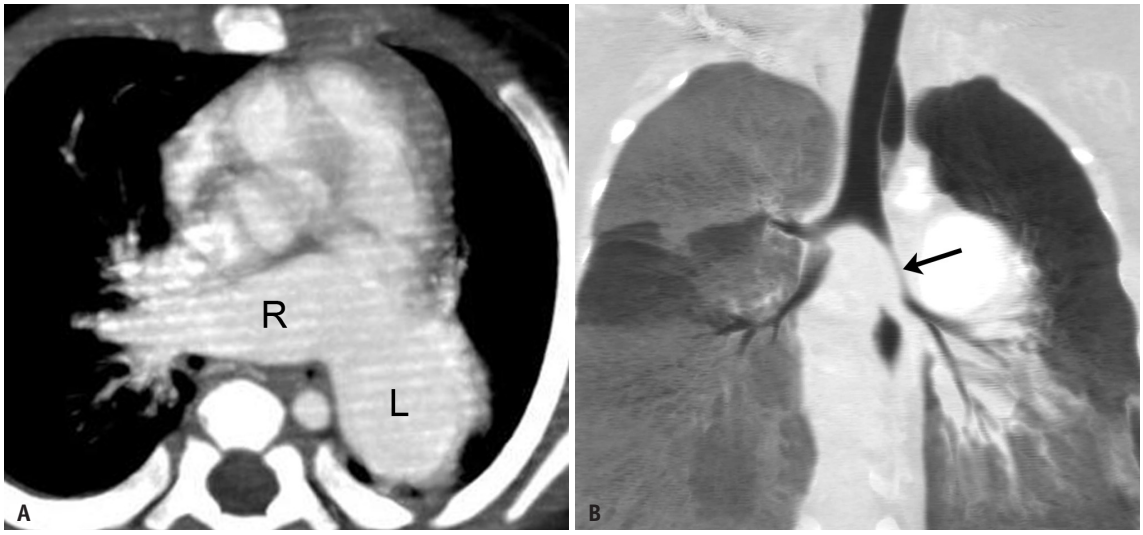

Fig. 4. Absent pulmonary valve syndrome in a 4-month-old girl.
A. Axial CT image with maximum intensity projection demonstrates the dilated right (R) and left (L) pulmonary arteries. **B.** Coronal CT image with minimum intensity projection shows central airway narrowings, most severely involving the left main bronchus (arrow) compressed by the dilated proximal branch pulmonary arteries. Hyperlucent lung areas due to air trapping are also noted.

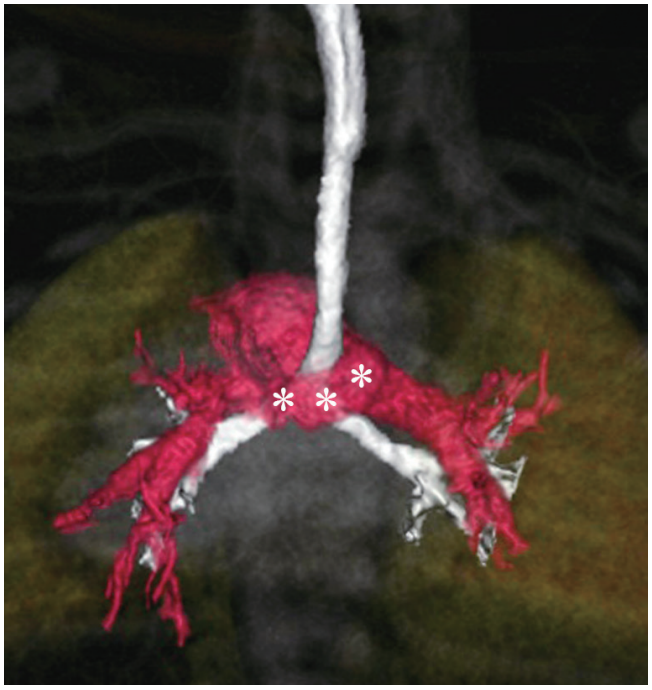

Fig. 5. Left pulmonary artery sling in a 6-month-old girl. Color-coded volume-rendered CT image with posterior view demonstrates left pulmonary artery sling (asterisks) and congenial tracheal stenosis (white).

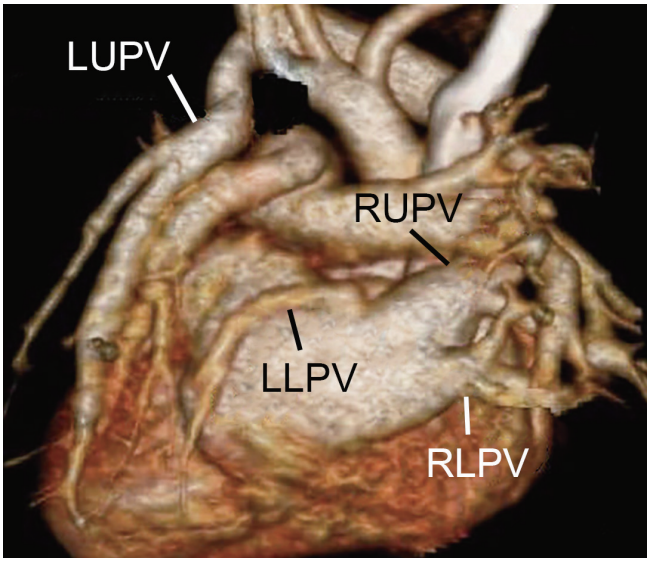

Fig. 6. Partial anomalous pulmonary venous return in a 5-month-old boy. Volume-rendered CT image with posterior view demonstrates that the LUPV anomalously drains into the innominate vein, whereas the other pulmonary veins are normally connected to the left atrium. Notably, the LLPV is diffusely small. LLPV = left lower pulmonary vein, LUPV = left upper pulmonary vein, RLPV = right lower pulmonary vein, RUPV = right upper pulmonary vein

vena cava.

In total anomalous pulmonary venous return (TAPVR), which is commonly associated with right atrial isomerism [23], the anomaly is classified into the supracardiac, cardiac (Fig. 7), infracardiac, and mixed types based on the location of the anomalous drainage [23,24]. When the infracardiac or mixed type is suspected on echocardiography, the upper abdominal region should be included in the scan range for cardiothoracic CT.

Anomalous pulmonary venous returns are frequently associated with atrial septal defect or patent foramen ovale [23,24]. Notably, CT is commonly used to identify PAPVR associated with sinus venosus defect (Fig. 8). PAPVR, or

https://doi.org/10.3348/kjr.2020.1332

Korean Journal of Radiology
KJR

rarely TAPVR, is one of anomalies constituting scimitar syndrome, which commonly involves the right lung [23].

CT is frequently used for the accurate and prompt diagnosis of congenital pulmonary vein obstruction [23,25,26]. Unilateral pulmonary vein atresia is usually asymptomatic and incidentally detected in most cases. In contrast, bilateral pulmonary vein atresia or common pulmonary vein atresia, although extremely rare, cannot be distinguished from obstructive TAPVR clinically, but it can be accurately diagnosed with CT [26].

CT is also useful for evaluating postoperative residual or recurrent pulmonary vein stenosis or occlusion (Fig. 9).

Aorta

Congenital anomalies of the aorta may occur in isolation or more commonly with other cardiac defects (especially involving the conotruncal region) and chromosomal abnormalities [27].

Supravalvular aortic stenosis may occur in association with or without Williams syndrome, and it may show

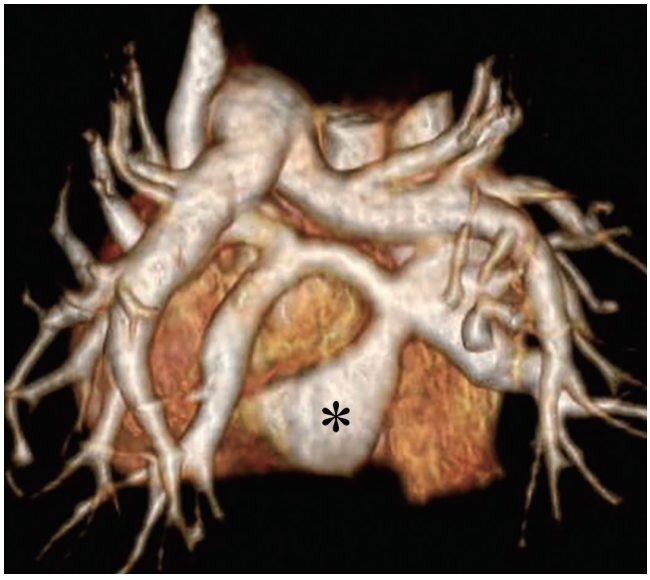

Fig. 7. Cardiac total anomalous pulmonary venous return in a 3-month-old boy. Volume-rendered CT image with posterior view reveals that all pulmonary veins anomalously drain into the dilated coronary sinus (asterisk).

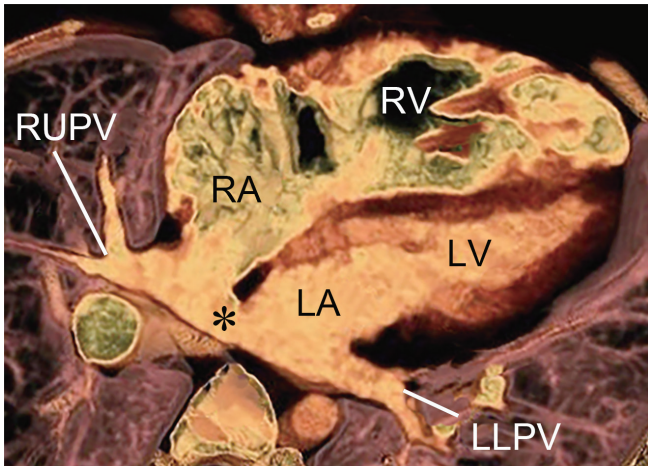

Fig. 8. Partial anomalous venous return and sinus venosus atrial septal defect in a 27-year-old woman. Transverse volume-rendered CT image shows that the RUPV anomalously drains into the RA, whereas the LLPV normally drains into the LA. A sinus venosus atrial septal defect (asterisk) is also seen. LA = left atrium, LLPV = left lower pulmonary vein, LV = left ventricle, RA = right atrium, RUPV = right lower pulmonary vein, RV = right ventricle

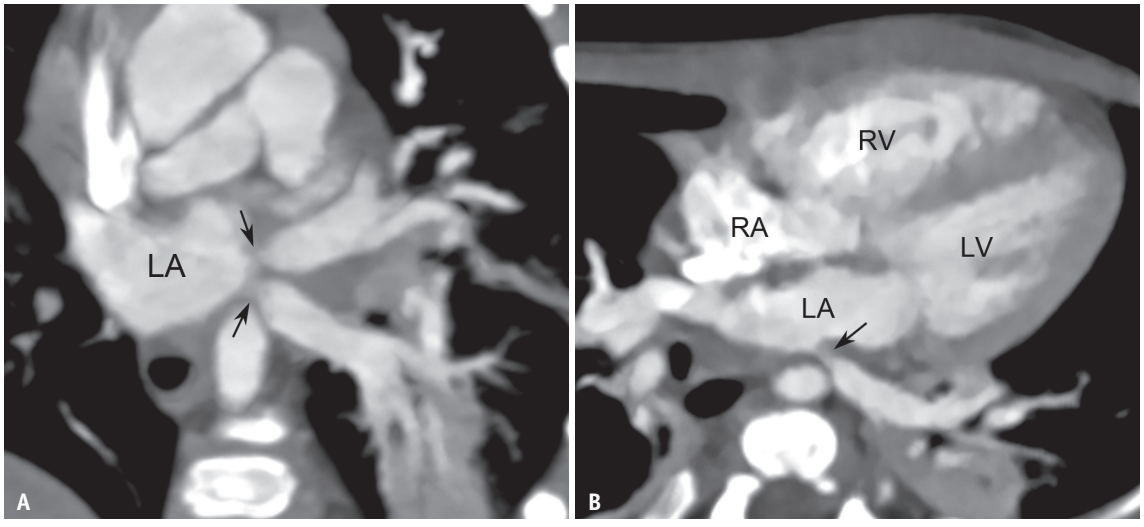

Fig. 9. Isolated pulmonary vein stenosis in a 5-momth-old girl.
A, B. Oblique coronal **(A)** and oblique axial **(B)** CT images reveal focal stenosis (arrows) of the left pulmonary yeins at the atrio-pulmonary venous junctions. LA = left atrium, LV = left ventricle, RA = right atrium, RV = right ventricle

https://doi.org/10.3348/kjr.2020.1332

a discrete narrowing (mimicking hourglass deformity), multiple stenoses, or diffuse hypoplasia on CT (Fig. 10) [28]. Coronary artery abnormalities, including ostial stenosis, diffuse stenosis, dilatation, and inflow obstruction by the aortic valve, the sinotubular ridge, or a combination of both, may be identified on CT [29]. CT is also useful for evaluating post-aortoplasty outcomes [30].

Coarctation of the aorta may present as a discrete juxtaductal stenosis, tubular arch hypoplasia, or a combination of both (Fig. 11) [31]. Interrupted aortic arch, defined as the loss of luminal continuity between the ascending and descending aorta, is divided into type A (distal to the left subclavian artery; most common in Asia), type B (between the left subclavian artery and left common carotid artery; most common in West), and type C (between the left common carotid artery and innominate artery; rare) according to the location of the interruption in the left arch [32]. In these two anomalies, CT can provide detailed aortic arch morphology, left ventricular outlet obstruction associated with posterior malalignment ventricular septal defect, combined cardiovascular defects, and the absence of the thymus in cases of DiGeorge syndrome [31,32]. Additionally, CT is useful for identifying post-treatment complications such as residual or recurrent aortic stenosis, dissection, and pseudoaneurysm (Fig. 12) [31,32].

A vascular ring encircling the trachea and esophagus may cause variable degrees of compression leading to respiratory symptoms and/or dysphagia [33]. The double aortic arch and the right aortic arch with an aberrant left subclavian

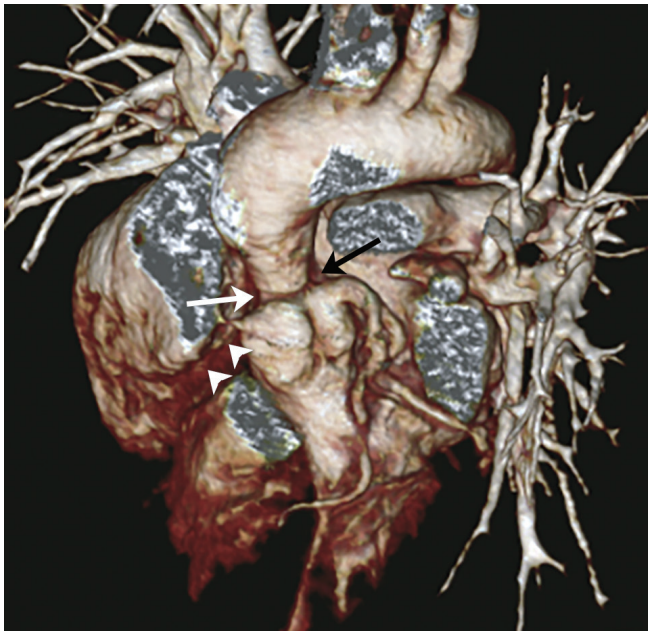

Fig. 10. Supravalvular aortic stenosis in a 13-year-old boy. Volume-rendered CT image demonstrates discrete supravalvular aortic stenosis (arrows) and the dilated and tortuous left coronary artery. In contrast, the right coronary artery is barely seen (arrowheads).

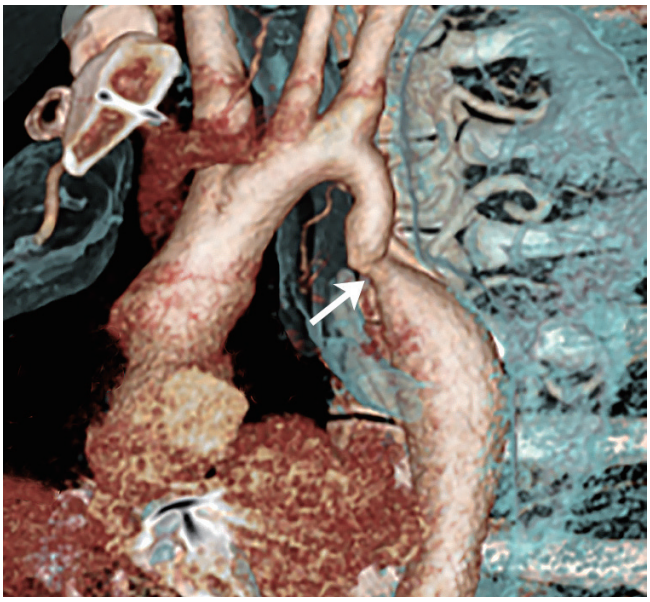

Fig. 11. Coarctation of the aorta in a 23-year-old man with systemic hypertension. Volume-rendered CT image with lateral view shows a discrete juxtaductal narrowing (arrow) and the mildly hypoplastic isthmus. Post-stenotic dilatation of the proximal descending aorta and dilated collateral arteries around the aortic lesion are noted.

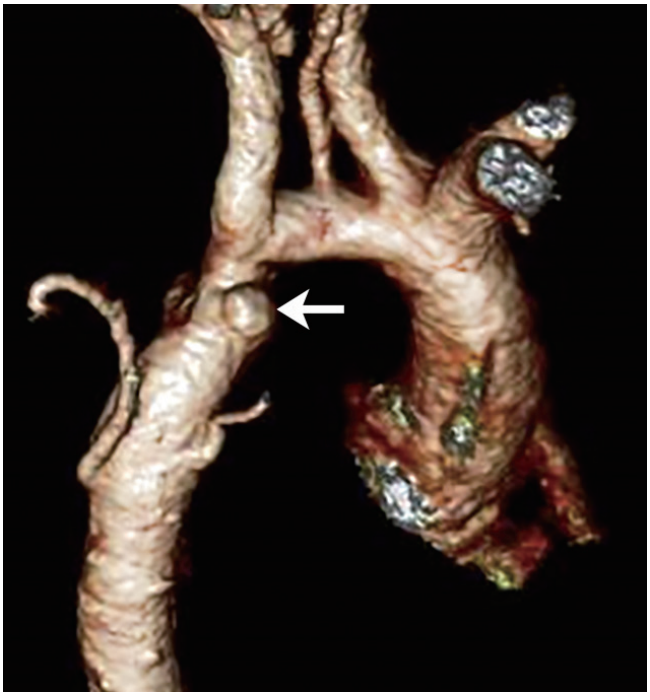

Fig. 12. Coarctation of the aorta in a 5-year-old girl who underwent balloon angioplasty. Volume-rendered CT image with oblique sagittal view performed 1 year after angioplasty demonstrates a pseudoaneurysm (arrow).

https://doi.org/10.3348/kjr.2020.1332

Korean Journal of Radiology
KJR

artery are the two most common vascular rings. CT is the imaging modality of choice for evaluating vascular airway compression and associated tracheomalacia [34-36]. In a double aortic arch, the right arch is commonly larger and higher than the left arch (Fig. 13). Less frequently, a distal portion of the smaller arch may be stenotic or atretic [37]. In an aberrant left subclavian artery, a PDA or ligamentum arteriosum completes the vascular ring. At its proximal portion, the Kommerell diverticulum may compress the adjacent airway and esophagus directly.

A persistent fifth aortic arch rarely originates from the distal ascending aorta, which is proximal and opposite to the ostium of the innominate artery and connects to the descending aorta. Typically, a persistent fifth aortic arch traverses under the normally developed fourth aortic arch, and these two arches show a superior-inferior relationship. Both arches may be patent (double-barreled or double-lumen aorta) or the superior arch may show atresia or interruption (Fig. 14) [38,39].

Rarely, pseudocoarctation demonstrates elongation and kinking of the aorta without a significant pressure gradient across the lesion or increased collateral circulation. Patients are usually asymptomatic, and they are followed up for a mild aortic coarctation. CT evaluation may be requested when significant flow acceleration is observed across this anomaly on Doppler echocardiography (Fig. 15) [40].

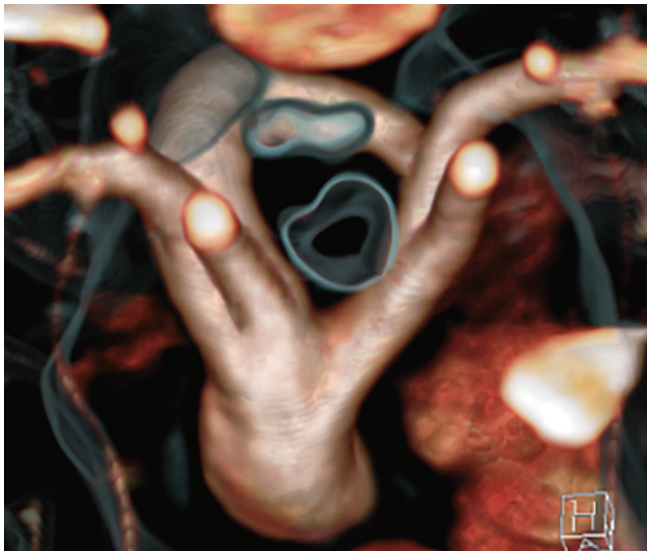

Fig. 13. Double aortic arch in a 6-month-old boy with persistent stridor since birth. Superior volume-rendered CT image shows double aortic arch with a dominant right arch. A bronchoscopy demonstrates tracheomalacia with abnormal vascular pulsation from the posterior wall.

Patent Ductus Arteriosus

CT may be used for the morphologic evaluation of a PDA before ductal stent placement in patients with ductal-dependent CHDs, such as tetralogy of Fallot and functional single ventricle with severe pulmonary stenosis or atresia and hypoplastic left heart syndrome (Fig. 16) [41]. CT may be useful for a tortuous or complex PDA that is not clearly delineated on echocardiography [42]. Moreover, CT may be used to detect stent-related complications, such as branch pulmonary artery narrowing, aortic narrowing, stent migration, and in-stent thrombosis. Similarly, CT may be used to assess complications after ductal device closure, such as device embolization or protrusion into the adjacent vasculature. Virtual angioscopy may help visualize an occlusion device from the inside from the aortic and pulmonary sides [43]. Of note, beam-hardening artifacts caused by the ductal implants may make accurate CT assessment difficult.

Coronary Artery

The use of pediatric coronary CT angiography is increasing due to improvements in coronary artery visibility [44-48]. Because young children have high heart rates and a limited ability to follow CT instructions, optimized

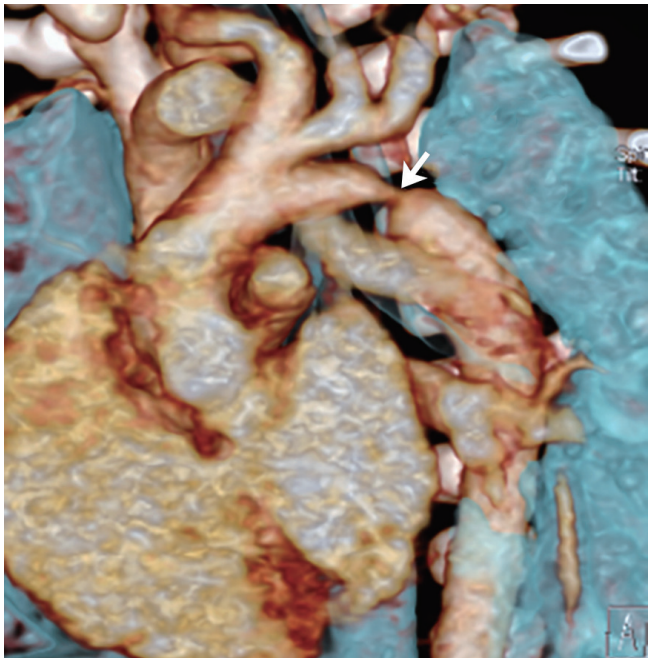

Fig. 14. Persistent fifth aortic arch in an 11-day-old girl. Volume-rendered CT image reveals coarctation (arrow) of a persistent fifth aortic arch and a type A interrupted fourth aortic arch.

https://doi.org/10.3348/kjr.2020.1332

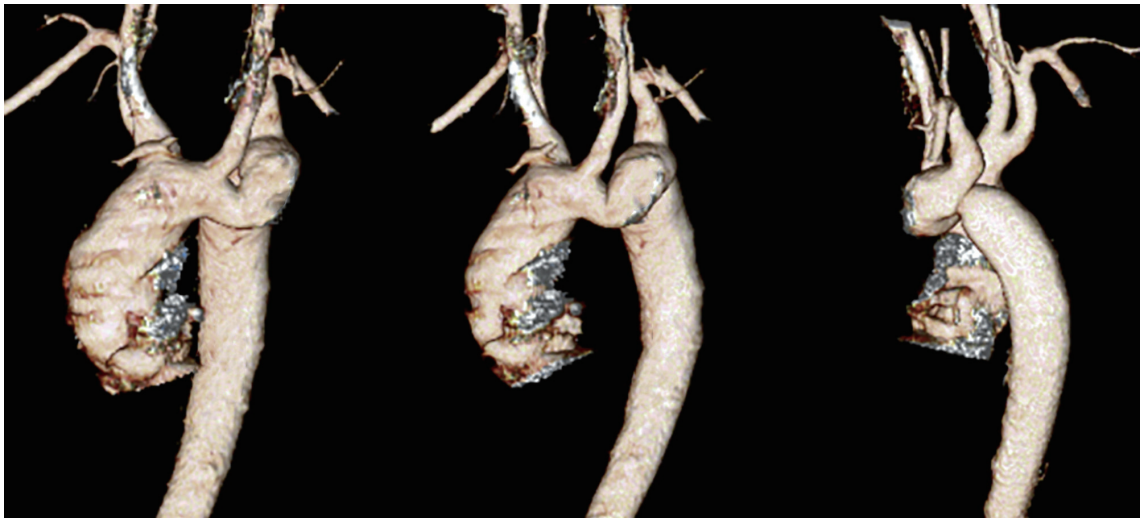

Fig. 15. Pseudocoarctation in an 18-year-old woman with Turner syndrome. A series of sagittal volume-rendered CT images of the aorta show the tortuous, elongated distal aortic arch with mild narrowing, which is consistent with pseudocoarctation. Cardiac catheterization confirmed no significant pressure gradients across the narrowing.

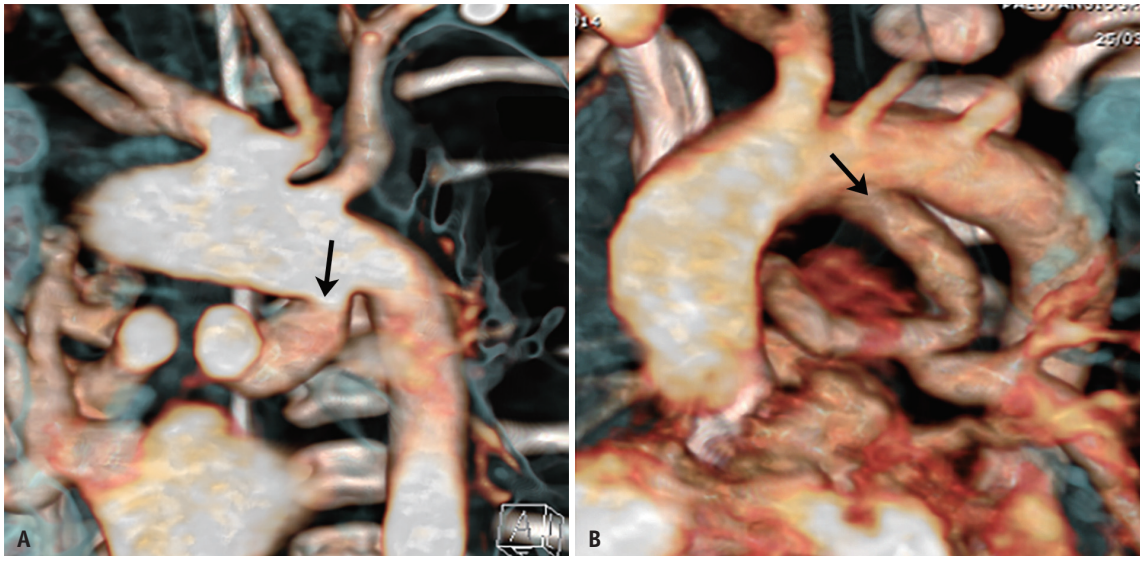

Fig. 16. Various origins of patent ductus arteriosus from the aorta.
A. Oblique coronal volume-rendered CT image obtained from a 28-day-old boy with tricuspid atresia and pulmonary atresia, shows a patent ductus arteriosus (arrow) originating from the distal aortic arch immediately distal to the left subclavian artery origin. **B.** Oblique coronal volume-rendered CT image obtained from a 7-day-old boy with pulmonary atresia and atrioventricular septal defect demonstrates a patent ductus arteriosus (arrow) arising from the proximal aortic arch opposite to the left common carotid artery origin. Various origins and courses of patent ductus arteriosus reflect the effect of ductal flow during fetal life on the development of ductal tissue. Accurate evaluation of morphologic features depicted on CT imaging helps plan ductal stent placement.

imaging techniques are important to evaluate coronary arteries [6,49].

Compared with that in the general population, the prevalence of coronary artery anomalies is higher (approximately 5–10%) in patients with CHD, and most of them are closely related to surgical techniques used for specific CHD, most commonly tetralogy of Fallot and transposition of the great arteries [10,50]. The CT-based incidence of coronary artery anomalies associated with tetralogy of Fallot has been reported to be 8.5–12.7%; the proportion of significant anomalies crossing the anterior aspect of the right ventricular outflow tract was 55.6–62.3% (Fig. 17) [51,52]. CT showed a high diagnostic accuracy of 91.7% for identifying various patterns of coronary artery anatomy before arterial switch operation in transposition of the great arteries [53]. Ventriculo-

https://doi.org/10.3348/kjr.2020.1332

Korean Journal of Radiology
KJR

coronary arterial communications are often observed in pulmonary atresia with an intact ventricular septum may lead to a right ventricle-dependent coronary circulation [54]. This fistulous connection can be identified on CT [55]. An anomalous origin of the left coronary artery from the pulmonary artery is a significant cause of acute heart failure in infants [56]. CT can be used to confirm the anomaly when echocardiographic findings are inconclusive [49]. The anomalous origin and course of the coronary arteries may lead to myocardial ischemia and sudden cardiac death, and a detailed morphologic spectrum of the anomaly can be accurately evaluated with CT for surgical planning [57]. Although an anomaly, such as high take-off coronary artery, may initially be hemodynamically minor, it may be considered as hemodynamically significant during cardiothoracic surgical or interventional procedures [10,58]. In addition, the coronary arteries may be compressed by adjacent anatomic structures or therapeutic implants.

Systemic Vein

The prevalence of a persistent left superior vena cava is higher in patients with CHD (up to 10%) than in the normal population (up to 0.5%) and much higher in patients with heterotaxy syndrome (up to 60–70%) [59]. A persistent left superior vena cava drains into the right atrium through a dilated coronary sinus. It may complicate catheter or pacemaker lead placement. Coronary sinus ostial atresia may be associated with a persistent left superior vena cava, and preoperative CT recognition of this rare anomaly is critically important in patients with a single functional ventricle [60]. The presence and size of a bridging vein between bilateral superior vena cavae should be noted on CT when planning a bidirectional cavopulmonary shunt.

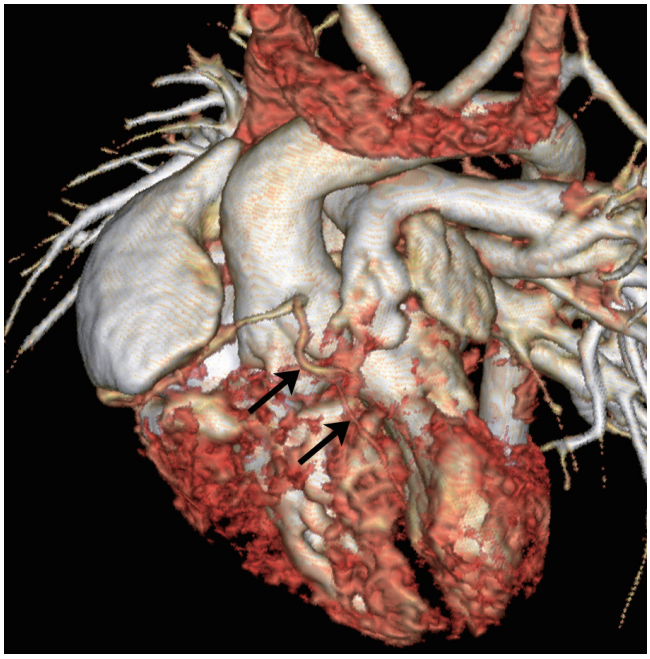

Fig. 17. Surgically significant coronary artery anatomy in a 3-month-old boy with tetralogy of Fallot. Volume-rendered CT image shows a left anterior descending artery (arrows) crossing the right ventricular outflow tract.

A levoatriocardinal vein is a form of pulmonary systemic connection most commonly observed in patients with left heart obstructive lesions [61]. It is important to differentiate a levoatriocardinal vein from more commonly encountered mimics, such as a vertical vein in an anomalous pulmonary venous return, a persistent left superior vena cava, and a dilated left superior intercostal vein [61]. Although the variant has no functional importance, a subaortic left innominate or brachiocephalic vein needs to be distinguished from the pulmonary artery and persistent left superior vena cava on preoperative CT in patients with CHD [62].

Interrupted inferior vena cava with azygos continuation is frequently (83%) observed in patients with left atrial isomerism [63]. In these patients, pulmonary arteriovenous malformations may be detected on CT in a lung with a deficient hepatic venous flow [64]. Separate hepatic venous drainage is often associated with heterotaxy syndrome (more frequently in right atrial isomerism), and it typically makes Fontan completion technically more difficult [65].

Cardiothoracic CT may be used to identify and monitor catheter-related thrombosis or stenosis in central thoracic veins in patients with CHD (Fig. 18), as demonstrated using CT venography in adults [66].

Ventricle

The morphologic left or right ventricle can be determined based on the presence of the moderator band, the degree of the trabeculations, and the septal attachment of the atrioventricular valve on CT [67]. In addition, abnormal ventriculoarterial and atrioventricular connections, such as a double-outlet right ventricle, discordant connections, a double-inlet left ventricle, and twisted connections, can be assessed with CT [8,67]. Clinically meaningful obstruction of the left or right ventricular outflow tract should be evaluated on end-systolic phase CT showing a minimal dimension [5,7]. In a double-chambered right ventricle, CT can reveal anomalous muscle bundles leading to the abnormal division

https://doi.org/10.3348/kjr.2020.1332

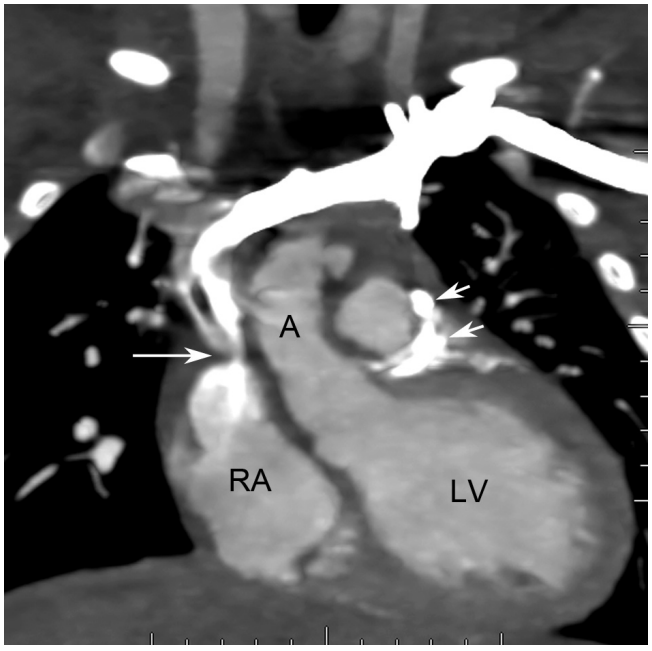

Fig. 18. Catheter-related systemic vein stenosis in a 3-month-old boy who underwent patch closure of ventricular septal defect and direct closure of patent foramen ovale. Coronal CT image reveals a focal stenosis (long arrow) at the junction between the superior vena cava and the RA. A contrast jet though the stenosis is seen in the RA. Undiluted contrast agent is opacified in the left pericardiacophrenic vein (short arrows), as a collateral vein, from the left brachiocephalic vein. A = ascending aorta, LV = left ventricle, RA = right atrium

of the right ventricle into a high-pressure inlet and a low-pressure outlet [68]. Pseudoaneurysm of the right ventricular outflow tract at the site of patch widening, as a rare postoperative complication, may be detected on CT after a total correction of tetralogy of Fallot [69]. A congenital cardiac ventricular diverticulum is rarely (3.4% for the left ventricle and 0.6% for the right ventricle) diagnosed using CT [70]. An apical diverticulum of the left ventricle and ectopia cordis may present in association with pentalogy of Cantrell [71]. Cardiothoracic CT may be used to characterize the type, size, number, and location of a ventricular septal defect [72]. In a double-outlet right ventricle, CT can show the intracardiac three-dimensional (3D) spatial relationships between a ventricular septal defect and the valves essential for surgical planning (Fig. 19) [73,74]. The transparent-lumen volume-rendering technique is useful for illustrating 3D morphologic features, especially the muscular type, of ventricular septal defects [75].

The degree of ventricular enlargement and hypertrophy resulting from volume and pressure loadings can be evaluated qualitatively on CT. Myocardial infarction may be demonstrated using myocardial delayed-enhancement CT

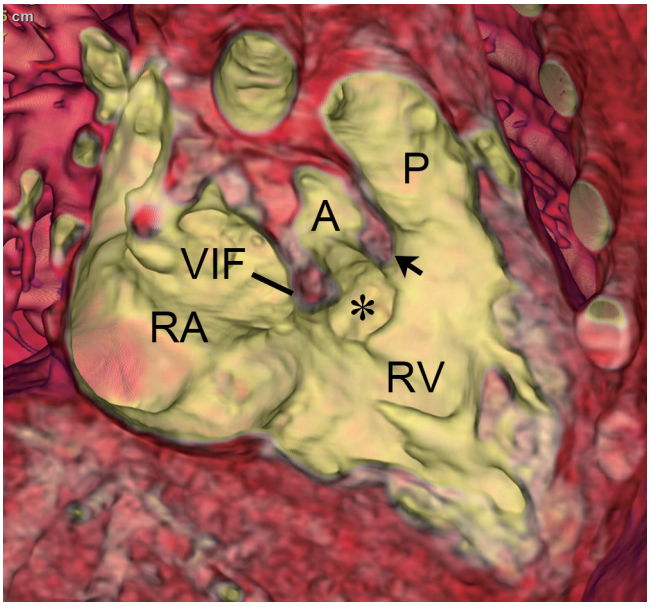

Fig. 19. Double-outlet RV with a ventricular septal defect in a 9-day-old girl. Oblique coronal transparent-lumen volume-rendered CT image with frontal cut demonstrates that a ventricular septal defect (asterisk), committed to the aortic valve and the outlet septum (arrow), is fused to the left margin of the ventricular septal defect. A short muscular subaortic stenosis is noted. A = ascending aorta, P = pulmonary trunk, RA = right atrium, RV = right ventricle, VIF = ventriculoinfundibular fold

imaging [76]. Furthermore, quantitative measures, including ventricular volume (Fig. 20A), myocardial mass (Fig. 20B), and myocardial strain, can be evaluated using CT in patients with CHD [77-82]. Based on a combined evaluation of CT-measured ventricular volume and mass, ventricular remodeling patterns, such as adaptation and maladaptation, may be assessed quantitatively [83].

Atrium

Unlike in other cardiovascular structures, it is challenging to obtain homogeneous contrast enhancement in the right atrium [84,85]. Slow injection of a contrast agent with a generous delay may help obtain homogeneous right atrial enhancement.

An atrial septal defect is classified into four types, including the secundum, primum, sinus venosus, and coronary sinus types. The secundum is the most common type, whereas the coronary sinus type is the rarest. The sinus venosus type is further divided into superior and inferior subtypes depending on whether the defect is close to the superior vena cava or inferior vena cava, respectively (Fig. 8). The coronary sinus type or unroofed coronary sinus is commonly associated with a persistent left superior vena

https://doi.org/10.3348/kjr.2020.1332

Korean Journal of Radiology
KJR

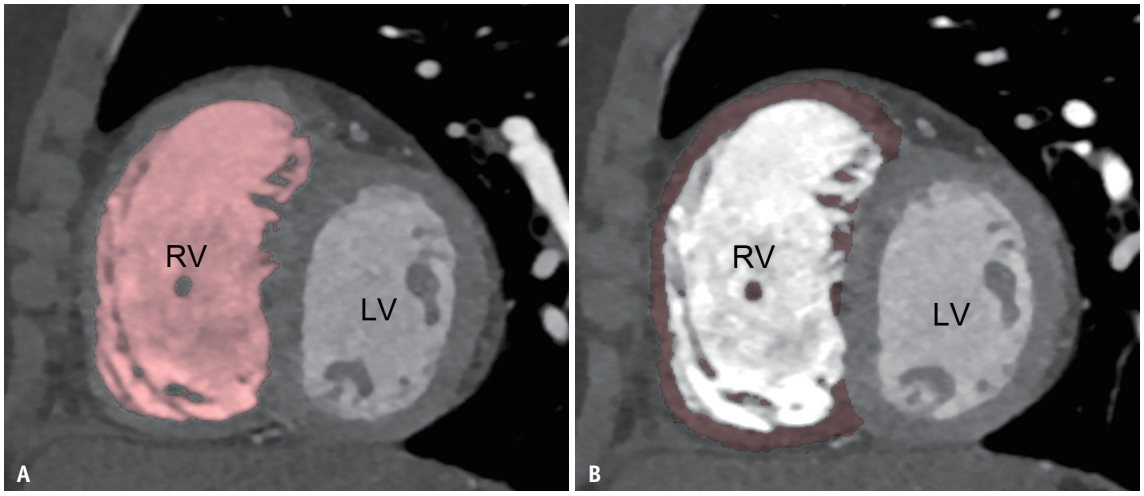

Fig. 20. Quantification of ventricular volume and myocardial mass in a 10-year-old girl with repaired tetralogy of Fallot.
A, B. Short-axis CT images obtained at the end-diastolic phase and the mid-ventricular level show the mildly enlarged RV (98.6 mL/m^2 of body surface area) with mild right ventricular hypertrophy (25.7 g/m^2 of body surface area). The right ventricular cavity (pink in **A**) and right ventricular myocardial mass (purple in **B**) were segmented using a three-dimensional threshold-based approach. LV = left ventricle, RV = right ventricle

cava [86,87]. Echocardiography is the mainstay diagnostic modality for evaluating atrial septal defect, particularly in the secundum and primum defects, because the interatrial septum is thin, and it may not always be discernible on CT. CT is mainly useful for the sinus venosus type, and it facilitates the determination of the subtype and the associated PAPVR, which is useful for surgical planning (closing an atrial septal defect and rerouting anomalous pulmonary venous flow into the left atrium [LA]). PAPVR commonly associated with the sinus venosus type of atrial septal defects may be missed on echocardiography. CT is also useful for delineating the location and extent of the coronary sinus type [88].

Cor triatriatum sinister is characterized by the division of the LA into proximal and distal chambers by a fibromuscular membrane located superior to the left atrial appendage [89]. The atrial septal defect, PAPVR, and mitral valvular disease are commonly associated with this anomaly. CT can depict the size and numbers of fenestrations in the fibromuscular membrane and its associated anomalies (Fig. 21) [90]. Because of the similar morphological and clinical characteristics, this anomaly should be distinguished from the supramitral valve ring, in which the obstructive ring is located inferior to the left atrial appendage.

Cor triariatum dexter is a rare anomaly in which the right atrium is divided into upstream and downstream chambers by a fibromuscular band. Imaging reveals a membrane coursing from the inferior vena cava to the superior vena cava, separating the right atrium into a posterior chamber (upstream), receiving vena caval flow and coronary sinus drainage, and an anterior chamber (downstream), containing the right atrial appendage and connecting the tricuspid valve [91].

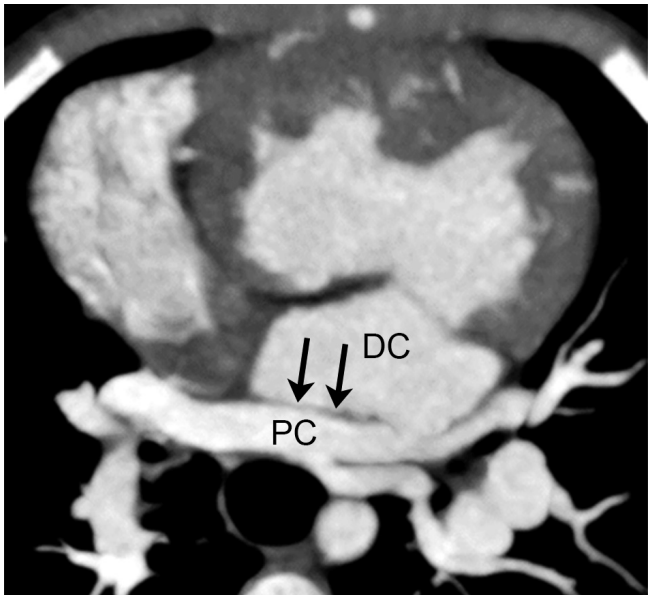

Fig. 21. Cor triatriatum sinister in a 4-year-old boy with double-outlet right ventricle. Axial CT image shows a membrane (arrows) dividing the left atrium into a PC and a DC. The pulmonary veins are connected to the PC and the left atrial appendage is connected to the DC. DC = distal chamber, PC = proximal chamber

Airway and Lung

CT is the imaging modality of choice for evaluating airway

https://doi.org/10.3348/kjr.2020.1332

anomalies and abnormalities commonly associated with CHD [92]. Vascular airway compression is frequently observed before and after cardiac surgery. The left main bronchus is frequently compressed between the descending thoracic aorta and a portion of the pulmonary artery and commonly associated with aortic arch repair [93]. The trachea is typically compressed by vascular rings and slings, including a double aortic arch (Fig. 14), right aortic arch with an aberrant left subclavian artery with or without Kommerell diverticulum, and pulmonary artery sling (Fig. 5) [94]. Tracheobronchomalacia, typically secondary to long-standing extrinsic vascular compression, can be detected with cine or four-dimensional CT [35,36,95]. Airway anomalies, such as tracheal bronchus [96], congenital tracheal stenosis (Fig. 5) [97], and bridging bronchus [22], are more frequently observed in patients with CHD, and they can be depicted accurately on CT. In heterotaxy syndrome, the anatomical relationship between the upper lobe bronchus and the pulmonary artery, which is the eparterial or hyparterial bronchus, on CT is useful for determining atrial situs [67,72].

CT can provide unprecedented lung imaging. In scimitar syndrome, various degrees of lung hypoplasia are associated with cardiac defects, most commonly ASD [98], and rarely the horseshoe lung, characterized by the fusion of the right and left lower lobes across the midline of the body [99]. Upper and lower airway obstructions frequently result in air trapping in young children with CHD. The extent of air trapping can be accurately identified on expiratory-phase CT imaging using mechanical or controlled ventilation with passive breath-holding at end-expiration [95,100] or the less invasive cine imaging technique during free breathing [101].

Heterotaxy Syndrome

Heterotaxy syndrome is a complex anomaly presenting with various congenital defects, including CHD and abnormal organ positions. This syndrome has two major categories consisting of bilateral right-sidedness and bilateral left-sidedness; the latter is rarer than the former. Using segmental analysis on CT, various abnormalities observed as part of this syndrome can be characterized [102,103].

In addition to the thorax, we should include the abdomen in the scan range of initial cardiothoracic CT to assess abdominal situs when abdominal sonography is not performed and planned for this assessment. The abdominal situs is likely ambiguous if a midline gallbladder is identified, and a horizontal liver and no spleen constitute the rule, which is consistent with asplenia syndrome closely associated with right atrial isomerism. In contrast, patients with polysplenia syndrome or left atrial isomerism usually have multiple small spleens and interrupted inferior vena cava with azygos continuation.

The morphologic characteristics of the atrial appendages are keys to determining the atrial situs [67]. Bronchopulmonary morphology on CT can also be used to suggest atrial situs: bilateral short and trifurcated bronchi with three lung lobes in right atrial isomerism and bilateral long and bifurcated bronchi with two lung lobes in left atrial isomerism.

When a bridging vein between the bilateral superior vena cavae is small or absent, cavopulmonary connections should be performed on both sides. TAPVR is commonly associated with right atrial isomerism. In heterotaxy syndrome, a morphological right ventricle is usually dominant, whereas a morphological left ventricle is generally underdeveloped.

Most patients with heterotaxy syndrome end up with a staged single ventricular repair [104]. Before and after surgical or interventional treatment, the adequacy of pulmonary flow can be monitored and quantified using CT [105]. To avoid heterogeneous enhancement in a Fontan pathway mimicking vascular stenosis or thrombosis after Fontan operation, contrast enhancement protocols should be carefully optimized [84,106]. Moreover, CT can demonstrate systemic venous collaterals between the upper and lower body parts as well as the systemic arterial collaterals to the lungs, which indicates the elevation of the pulmonary arterial pressure often leading to Fontan failure [107]. Systemic to pulmonary venous collaterals leading to arterial desaturation may also be identified on CT (Fig. 22) [108]. However, cardiac MRI is more frequently used for the comprehensive evaluations of the Fontan pathway.

Valve

CT is not used as a primary diagnostic imaging method for evaluating cardiac valves mainly due to its insufficient temporal and spatial resolutions and high radiation exposure required for data acquisition throughout the entire cardiac cycle. Nevertheless, CT may be used for morphologic and functional assessments of cardiac valves in patients with CHD [109]. The number of the semilunar valve leaflets may be evaluated on CT. Valve thickening and doming with restricted opening on CT suggest the presence of valvular

https://doi.org/10.3348/kjr.2020.1332

Korean Journal of Radiology
KJR

stenosis (Fig. 23). In valvular insufficiency, valve cusps fail to coapt during diastole. In muscular pulmonary atresia, the sizable infundibulum and the distance between the main pulmonary artery and the infundibulum can be accurately assessed with CT. CT may be used for the postsurgical comprehensive assessment of prosthetic heart valves [110]. In children, longitudinal coverage of multi-phase CT scanning should be minimized to reduce CT radiation dose (Fig. 24). CT can be used for evaluating commissural malalignment of the semilunar valves in patients with transposition of the great arteries frequently requiring modified coronary transfer techniques during an arterial

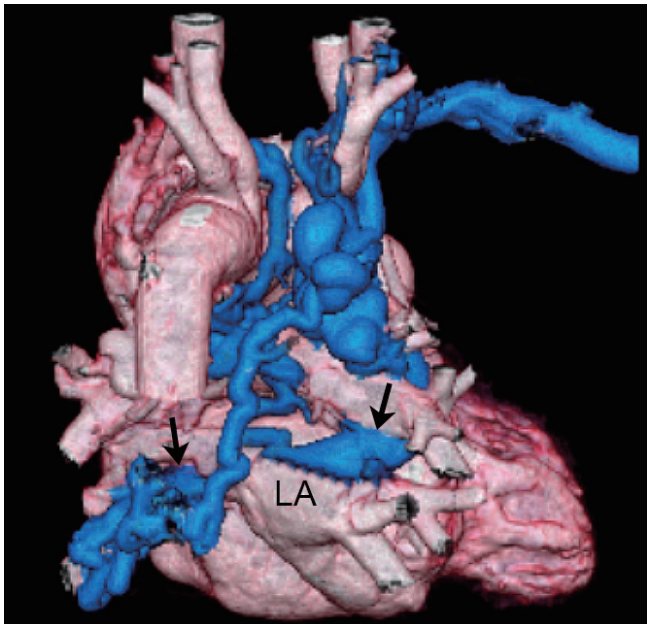

Fig. 22. Systemic to pulmonary venous collaterals in a 10-year-old girl with desaturation who underwent Fontan operation.
Volume-rendered CT image with oblique posterior view shows dilated systemic venous collaterals (blue) draining into the LA directly or via the pulmonary veins (arrows). After the coil embolization of these systemic to pulmonary venous collaterals, oxygen saturation was increased. The patient has dextrocardia and a right aortic arch. LA = left atrium

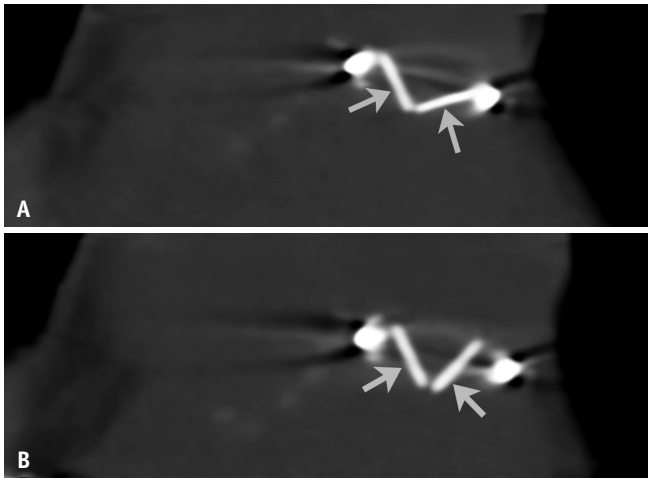

Fig. 24. CT assessment of prosthetic valve motion in a 14-year-old boy with tetralogy of Fallot who underwent total correction and pulmonary valve replacement.
A, B. Oblique coronal diastolic **(A)** and systolic **(B)** unenhanced CT images obtained with a minimal longitudinal scan range demonstrate a bi-leaflet prosthetic pulmonary valve (arrows) with the valve in closed **(A)** and open **(B)** position. Two leaflets show severely limited opening during systole **(B)**, which is more severe on the right side. Based on the CT finding, urokinase was administered for 72 hours to treat the prosthetic valve malfunction.

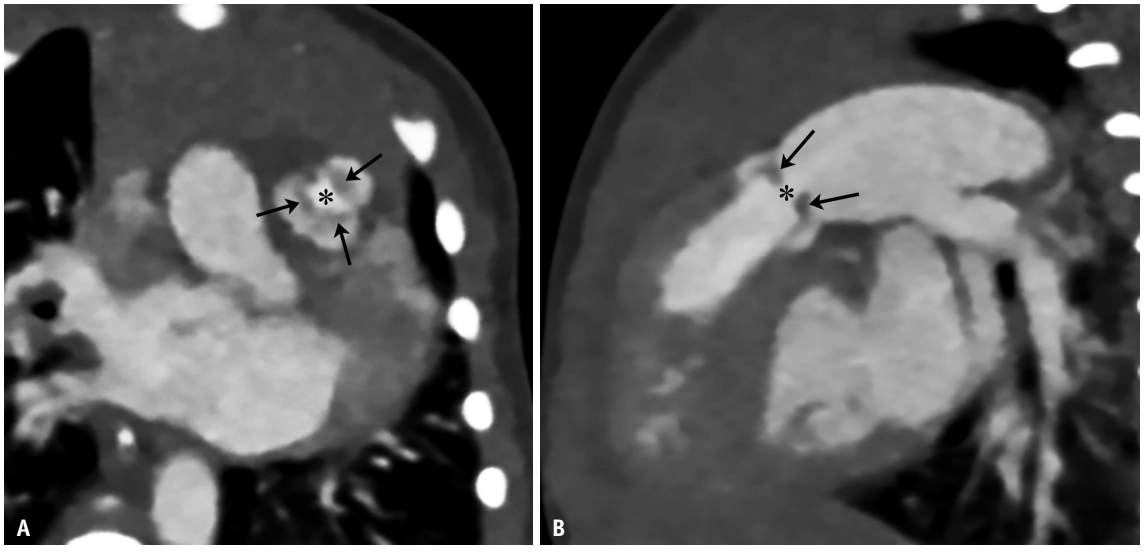

Fig. 23. Valvular pulmonary stenosis in a 4-day-old boy.
A, B. Oblique axial **(A)** and oblique sagittal **(B)** CT images show thickening and doming of the pulmonary valve leaflets (arrows) and restricted valve opening (asterisks) during systole.

https://doi.org/10.3348/kjr.2020.1332

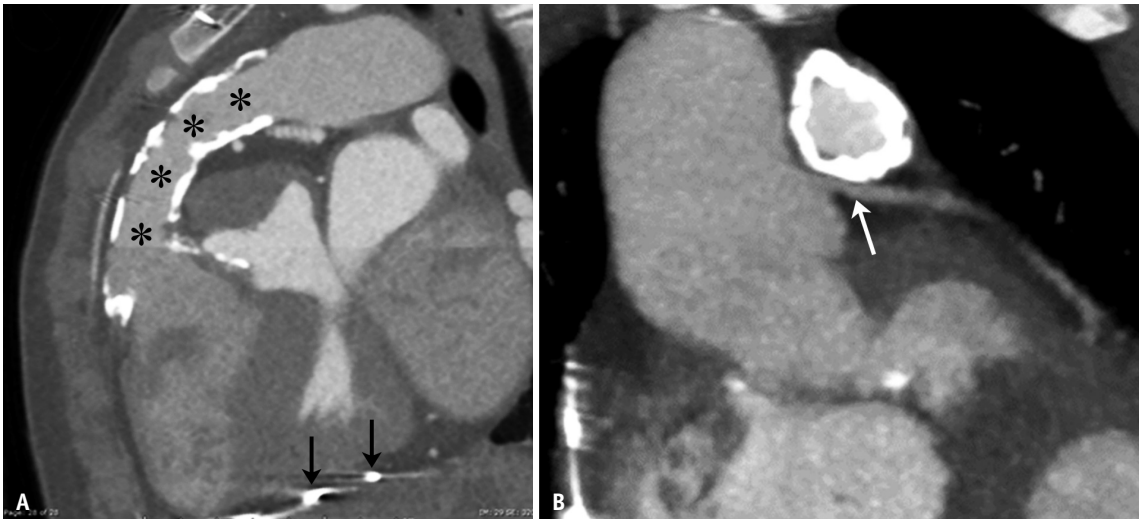

Fig. 25. RV-PA conduit in a 14-year-old boy with transposition of the great arteries, ventricular septal defect, and pulmonary stenosis who underwent Rastelli operation.
A. Sagittal CT image shows extensive calcific degeneration of an RV-PA conduit (asterisks). Pacing wire is noted (arrows). **B.** Short-axis CT image shows proximity of the left coronary artery (arrow) and the conduit. PA = pulmonary artery, RV = right ventricle

switch operation [111].

The anatomic and functional assessment of the atrioventricular valves in CHD is primarily performed with echocardiography. A muscular type of tricuspid or mitral atresia can be observed on CT [7], but a membrane type of atrioventricular valve atresia may not be distinguished from the non-atretic atrioventricular valve on CT. In addition, detailed morphologic features of atrioventricular valve abnormalities in the atrioventricular septal defect cannot be evaluated with CT. In a hypoplastic ventricle, CT-based morphometric measures (i.e., diameter and area) of the small atrioventricular valve annulus may be used to plan an optimal surgical strategy [112]. The displaced and tethered tricuspid valve in Ebstein anomaly may be identified on CT [7,8]. Volumetric severity assessment using CT was recently reported to be feasible and useful for characterizing various phenotypes of this anomaly [113].

Table 1. Contemporary Clinical Applications of Pediatric Cardiothoracic CT

Essential	Evaluation of extracardiac vasculatures
	Airway and lungs
	Mediastinum and bony thorax
	Vascular shunt, stent, and conduit
	Comorbid anomalies associated with heterotaxy syndrome
	Postoperative complications
	Pericardium
Optional	Intracardiac structures
	Coronary artery
	Valvular morphology and motion
	Quantitative and functional analysis
	Surgical/interventional simulation
	Myocardial perfusion and infarction
	Diaphragm

Typically, the essential evaluations are almost always included in every cardiothoracic CT examination and can be promptly completed, while the optional evaluations are performed as needed and take more time and effort.

Vascular Shunt, Conduit, Baffle, and Vascular Stent

Cyanotic CHDs are commonly associated with small pulmonary artery size and flow. Therefore, a palliative procedure is performed to promote pulmonary arterial growth before corrective surgery. In this respect, a vascular shunt is commonly created for that purpose by connecting the aorta (a central shunt) or its branch (usually the subclavian artery; a modified Blalock–Taussig shunt) to the pulmonary artery. CT is useful for monitoring pulmonary arterial growth and evaluating potential complications, including shunt thrombosis or stenosis, calcified wall graft, seroma around the shunt, and retraction and stenosis of the pulmonary artery around the shunt insertion [114].

A conduit and a baffle are used for redirecting blood flow in complex CHD. A conduit (frequently containing a valve) is used for extracardiac rerouting of blood flow in outflow tract or semilunar valve obstruction, whereas a baffle is used for intracardiac flow rerouting [115]. A conduit

https://doi.org/10.3348/kjr.2020.1332

Korean Journal of Radiology
KJR

connecting the right ventricle and the pulmonary artery, the so-called Rastelli procedure, is commonly used for tetralogy of Fallot with pulmonary atresia, transposition of the great artery, and severe left ventricular outflow tract obstruction. In addition to the evaluation of conduit patency and complications, CT may be used for evaluating retrosternal proximity of the conduit and close proximity of the conduit to the coronary artery to prevent serious vascular injury during redo surgery or interventional treatment (Fig. 25).

For evaluating an implanted vascular stent, CT is the imaging method of choice [116] because MRI is considerably limited in assessing vascular stents due to ferromagnetic metallic artifacts.

Summary

To achieve appropriate managements for patients with CHD, anatomical and hemodynamic information is necessary. Currently, CT can provide accurate anatomical information and some quantitative information quickly, which is useful for expeditious management decisions. Advanced 3D visualization techniques, such as augmented reality, virtual reality, and 3D printing, using 3D cardiothoracic CT data have been widely used in CHD for education, preprocedural planning and simulation, procedural guidance, and development of new insights in embryology and pathology of complex cardiac defects [75,117]. This comprehensive review includes a wide spectrum of contemporary organ-based clinical applications of pediatric cardiothoracic CT for different types of CHD (Table 1). The organ-based approach demonstrated in this review is more effective and more practical in evaluating CHD cases in which the primary diagnosis is typically made with echocardiography. Pediatric cardiothoracic CT is typically requested to specify which organs need to be assessed. In this regard, CT provides complimentary but important information about cardiac and extracardiac structures, which cannot be clearly answered using echocardiography or catheter angiography.

Conflicts of Interest

The authors have no potential conflicts of interest to disclose.

Author Contributions

Conceptualization: Hyun Woo Goo, Suvipaporn Siripornpitak, Shyh-Jye Chen, Oktavia Lilyasari, Yu-Min Zhong, Haifa Abdul Latiff, Eriko Maeda. Data curation: Hyun Woo Goo. Methodology: all authors. Project administration: Hyun Woo Goo. Supervision: Hyun Woo Goo. Validation: all authors. Visualization: Hyun Woo Goo, Suvipaporn Siripornpitak, Shyh-Jye Chen, Oktavia Lilyasari, Yu-Min Zhong, Haifa Abdul Latiff. Writing—original draft: Hyun Woo Goo, Suvipaporn Siripornpitak, Shyh-Jye Chen, Oktavia Lilyasari, Yu-Min Zhong, Haifa Abdul Latiff. Writing—review & editing: Hyun Woo Goo, Eriko Maeda, Young Jin Kim, I-Chen Tsai, Dong Man Seo.

ORCID iDs

Hyun Woo Goo
https://orcid.org/0000-0001-6861-5958
Suvipaporn Siripornpitak
https://orcid.org/0000-0002-4140-6280
Shyh-Jye Chen
https://orcid.org/0000-0001-6181-011X
Oktavia Lilyasari
https://orcid.org/0000-0003-3802-4801
Yu-Min Zhong
https://orcid.org/0000-0002-0164-8752
Haifa Abdul Latiff
https://orcid.org/0000-0001-5806-9113
Eriko Maeda
https://orcid.org/0000-0003-2123-9187
Young Jin Kim
https://orcid.org/0000-0002-6235-6550
I-Chen Tsai
https://orcid.org/0000-0002-4356-918X
Dong Man Seo
https://orcid.org/0000-0002-5831-7954

REFERENCES

1. Yang JC, Lin MT, Jaw FS, Chen SJ, Wang JK, Shih TT, et al. Trends in the utilization of computed tomography and cardiac catheterization among children with congenital heart disease. *J Formos Med Assoc* 2015;114:1061-1068
2. Lee T, Tsai IC, Fu YC, Jan SL, Wang CC, Chang Y, et al. Using multidetector-row CT in neonates with complex congenital heart disease to replace diagnostic cardiac catheterization for anatomical investigation: initial experiences in technical and clinical feasibility. *Pediatr Radiol* 2006;36:1273-1282
3. Hui PKT, Goo HW, Du J, Ip JJK, Kanzaki S, Kim YJ, et al. Asian consortium on radiation dose of pediatric cardiac CT (ASCI-REDCARD). *Pediatr Radiol* 2017;47:899-910
4. Goo HW. State-of-the-art CT imaging techniques for congenital heart disease. *Korean J Radiol* 2010;11:4-18
5. Goo HW. Cardiac MDCT in children: CT technology overview

 https://doi.org/10.3348/kjr.2020.1332

and interpretation. *Radiol Clin North Am* 2011;49:997-1010
6. Hong SH, Goo HW, Maeda E, Choo KS, Tsai IC; Asian Society of Cardiovascular Imaging Congenital Heart Disease Study Group. User-friendly vendor-specific guideline for pediatric cardiothoracic computed tomography provided by the Asian Society of Cardiovascular Imaging Congenital Heart Disease Study Group: part 1. Imaging techniques. *Korean J Radiol* 2019;20:190-204
7. Goo HW, Park IS, Ko JK, Kim YH, Seo DM, Yun TJ, et al. CT of congenital heart disease: normal anatomy and typical pathologic conditions. *Radiographics* 2003;23 Spec No:S147-S165
8. Goo HW, Park IS, Ko JK, Kim YH, Seo DM, Park JJ. Computed tomography for the diagnosis of congenital heart disease in pediatric and adult patients. *Int J Cardiovasc Imaging* 2005;21:347-365
9. Goo HW. Current trends in cardiac CT in children. *Acta Radiol* 2013;54:1055-1062
10. Goo HW, Seo DM, Yun TJ, Park JJ, Park IS, Ko JK, et al. Coronary artery anomalies and clinically important anatomy in patients with congenital heart disease: multislice CT findings. *Pediatr Radiol* 2009;39:265-273
11. Han BK, Rigsby CK, Hlavacek A, Leipsic J, Nicol ED, Siegel MJ, et al. Computed tomography imaging in patients with congenital heart disease part I: rationale and utility. An expert consensus document of the Society of Cardiovascular Computed Tomography (SCCT): endorsed by the Society of Pediatric Radiology (SPR) and the North American Society of Cardiac Imaging (NASCI). *J Cardiovasc Comput Tomogr* 2015;9:475-492
12. Tsai IC, Goo HW. Cardiac CT and MRI for congenital heart disease in Asian countries: recent trends in publication based on a scientific database. *Int J Cardiovasc Imaging* 2013;29 Suppl 1:1-5
13. Zucker EJ. Cross-sectional imaging of congenital pulmonary artery anomalies. *Int J Cardiovasc Imaging* 2019;35:1535-1548
14. Escalon JG, Browne LP, Bang TJ, Restrepo CS, Ocazionez D, Vargas D. Congenital anomalies of the pulmonary arteries: an imaging overview. *Br J Radiol* 2019;92:20180185
15. Lapierre C, Dubois J, Rypens F, Raboisson MJ, Déry J. Tetralogy of Fallot: preoperative assessment with MR and CT imaging. *Diagn Interv Imaging* 2016;97:531-541
16. Goo HW. Computed tomography pulmonary vascular volume ratio in children and young adults with congenital heart disease: the effect of cardiac phase. *Pediatr Radiol* 2018;48:915-922
17. Meinel FG, Huda W, Schoepf UJ, Rao AG, Cho YJ, Baker GH, et al. Diagnostic accuracy of CT angiography in infants with tetralogy of Fallot with pulmonary atresia and major aortopulmonary collateral arteries. *J Cardiovasc Comput Tomogr* 2013;7:367-375
18. Lin MT, Wang JK, Chen YS, Lee WJ, Chiu HH, Chen CA, et al. Detection of pulmonary arterial morphology in tetralogy of Fallot with pulmonary atresia by computed tomography: 12 years of experience. *Eur J Pediatr* 2012;71:579-586
19. Koplay M, Cimen D, Sivri M, Güvenc O, Arslan D, Nayman A, et al. Truncus arteriosus: diagnosis with dual-source computed tomography angiography and low radiation dose. *World J Radiol* 2014;6:886-889
20. Yakut K, Tokel NK, Özkan M, Varan B, Erdoğan İ, Aşlamacı S. Diagnosis and surgical treatment of aortopulmonary window: our single-center experience. *Turk Gogus Kalp Damar Cerrahisi Derg* 2018;26:30-37
21. Zhong YM, Jaffe RB, Liu JF, Sun AM, Gao W, Wang Q, et al. Multi-slice computed tomography assessment of bronchial compression with absent pulmonary valve. *Pediatr Radiol* 2014;44:803-809
22. Zhong YM, Jaffe RB, Zhu M, Gao W, Sun AM, Wang Q. CT assessment of tracheobronchial anomaly in left pulmonary artery sling. *Pediatr Radiol* 2010;40:1755-1762
23. Dillman JR, Yarram SG, Hernandez RJ. Imaging of pulmonary venous developmental anomalies. *AJR Am J Roentgenol* 2009;192:1272-1285
24. Pandey NN, Sharma A, Jagia P. Imaging of anomalous pulmonary venous connections by multidetector CT angiography using third-generation dual source CT scanner. *Br J Radiol* 2018;91:20180298
25. Ou P, Marini D, Celermajer DS, Agnoletti G, Vouhé P, Sidi D, et al. Non-invasive assessment of congenital pulmonary vein stenosis in children using cardiac-non-gated CT with 64-slice technology. *Eur J Radiol* 2009;70:595-599
26. Goo HW, Park SH, Koo HJ, Cho YH, Lee E. Atresia of the bilateral pulmonary veins: a rare and dismal anomaly identified on cardiac CT. *Pediatr Radiol* 2014;44:942-947
27. Hanneman K, Newman B, Chan F. Congenital variants and anomalies of the aortic arch. *Radiographics* 2017;37:32-51
28. Liu PS, St John Sutton MG, Litt HI. Diffuse supravalvular aortic stenosis: comprehensive imaging with ECG-gated CT angiography. *Int J Cardiovasc Imaging* 2007;23:269-272
29. Das KM, Momenah TS, Larsson SG, Jadoon S, Aldosary AS, Lee EY. Williams-Beuren syndrome: computed tomography imaging review. *Pediatr Cardiol* 2014;35:1309-1320
30. Shin HJ, Jhang WK, Park JJ, Goo HW, Seo DM. Modified simple sliding aortoplasty for preserving the sinotubular junction without using foreign material for congenital supravalvar aortic stenosis. *Eur J Cardiothorac Surg* 2011;40:598-602
31. Karaosmanoglu AD, Khawaja RD, Onur MR, Kalra MK. CT and MRI of aortic coarctation: pre- and postsurgical findings. *AJR Am J Roentgenol* 2015;204:W224-W233
32. Yang DH, Goo HW, Seo DM, Yun TJ, Park JJ, Park IS, et al. Multislice CT angiography of interrupted aortic arch. *Pediatr Radiol* 2008;38:89-100
33. Tola H, Ozturk E, Yildiz O, Erek E, Haydin S, Turkvatan A, et al. Assessment of children with vascular ring. *Pediatr Int* 2017;59:134-140
34. Lee EY, Zurakowski D, Waltz DA, Mason KP, Riaz F, Ralph A,

https://doi.org/10.3348/kjr.2020.1332

et al. MDCT evaluation of the prevalence of tracheomalacia in children with mediastinal aortic vascular anomalies. *J Thorac Imaging* 2008;23:258-265
35. Goo HW. Free-breathing cine CT for the diagnosis of tracheomalacia in young children. *Pediatr Radiol* 2013;43:922-928
36. Goo HW. Four-dimensional thoracic CT in free-breathing children. *Korean J Radiol* 2019;20:50-57
37. Schlesinger AE, Krishnamurthy R, Sena LM, Guillerman RP, Chung T, DiBardino DJ, et al. Incomplete double aortic arch with atresia of the distal left arch: distinctive imaging appearance. *AJR Am J Roentgenol* 2005;184:1634-1639
38. Bernasconi A, Goo HW, Yoo SJ. Double-barrelled aorta with tetralogy of Fallot and pulmonary atresia. *Cardiol Young* 2007;17:98-101
39. Naimo PS, Vazquez-Alvarez Mdel C, d'Udekem Y, Jones B, Konstantinov IE. Double-lumen aortic arch: persistence of the fifth aortic arch. *Ann Thorac Surg* 2016;101:e155-e156
40. Thodi Ramamurthy M, Balakrishnan VK, David SAN, Korrapati HS. Congenital kinking of aorta. *BMJ Case Rep* 2017;2017:bcr2017220896
41. Jadhav SP, Aggarwal V, Masand PM, Diaz E, Zhang W, Qureshi AM. Correlation of ductus arteriosus length and morphology between computed tomographic angiography and catheter angiography and their relation to ductal stent length. *Pediatr Radiol* 2020;50:800-809
42. Rehman R, Marhisham MC, Alwi M. Stenting the complex patent ductus arteriosus in tetralogy of Fallot with pulmonary atresia: challenges and outcomes. *Future Cardiol* 2018;14:55-73
43. Hayabuchi Y, Mori K, Kagami S. Virtual endoscopy using multidetector-row CT for coil occlusion of patent ductus arteriosus. *Catheter Cardiovasc Interv* 2007;70:434-439
44. Goo HW, Yang DH. Coronary artery visibility in free-breathing young children with congenital heart disease on cardiac 64-slice CT: dual-source ECG-triggered sequential scan vs. single-source non-ECG-synchronized spiral scan. *Pediatr Radiol* 2010;40:1670-1680
45. Paul JF, Rohnean A, Elfassy E, Sigal-Cinqualbre A. Radiation dose for thoracic and coronary step-and-shoot CT using a 128-slice dual-source machine in infants and small children with congenital heart disease. *Pediatr Radiol* 2011;41:244-249
46. Kanie Y, Sato S, Tada A, Kanazawa S. Image quality of coronary arteries on non-electrocardiography-gated high-pitch dual-source computed tomography in children with congenital heart disease. *Pediatr Cardiol* 2017;38:1393-1399
47. Barrera CA, Otero HJ, White AM, Saul D, Biko DM. Depiction of the native coronary arteries during ECG-triggered high-pitch dual-source coronary computed tomography angiography in children: determinants of image quality. *Clin Imaging* 2018;52:240-245
48. Goo HW. Image quality and radiation dose of high-pitch dual-source spiral cardiothoracic computed tomography in young children with congenital heart disease: comparison of non-electrocardiography synchronization and prospective electrocardiography triggering. *Korean J Radiol* 2018;19:1031-1041
49. Goo HW. Coronary artery imaging in children. *Korean J Radiol* 2015;16:239-250
50. Lowry AW, Olabiyi OO, Adachi I, Moodie DS, Knudson JD. Coronary artery anatomy in congenital heart disease. *Congenit Heart Dis* 2013;8:187-202
51. Kervancioglu M, Tokel K, Varan B, Yildirim SV. Frequency, origins and courses of anomalous coronary arteries in 607 Turkish children with tetralogy of Fallot. *Cardiol J* 2011;18:546-551
52. Goo HW. Coronary artery anomalies on preoperative cardiac CT in children with tetralogy of Fallot or Fallot type of double outlet right ventricle: comparison with surgical findings. *Int J Cardiovasc Imaging* 2018;34:1997-2009
53. Goo HW. Identification of coronary artery anatomy on dual-source cardiac computed tomography before arterial switch operation in newborns and young infants: comparison with transthoracic echocardiography. *Pediatr Radiol* 2018;48:176-185
54. Giglia TM, Mandell VS, Connor AR, Mayer JE Jr, Lock JE. Diagnosis and management of right ventricle-dependent coronary circulation in pulmonary atresia with intact ventricular septum. *Circulation* 1992;86:1516-1528
55. Séguéla PE, Houyel L, Loget P, Piot JD, Paul JF. Critical stenosis of a right ventricle to coronary artery fistula seen at dual-source CT in a newborn with pulmonary atresia and intact ventricular septum. *Pediatr Radiol* 2011;41:1069-1072
56. Peña E, Nguyen ET, Merchant N, Dennie C. ALCAPA syndrome: not just a pediatric disease. *Radiographics* 2009;29:553-565
57. Pandey NN, Sinha M, Sharma A, Rajagopal R, Bhambri K, Kumar S. Anomalies of coronary artery origin: evaluation on multidetector CT angiography. *Clin Imaging* 2019;57:87-98
58. Tsai WL, Wei HJ, Tsai IC. High-take-off coronary artery: a haemodynamically minor, but surgically important coronary anomaly. *Pediatr Radiol* 2010;40:232-233
59. Batouty NM, Sobh DM, Gadelhak B, Sobh HM, Mahmoud W, Tawfik AM. Left superior vena cava: cross-sectional imaging overview. *Radiol Med* 2020;125:237-246
60. Kim C, Goo HW, Yu JJ, Yun TJ. Coronary sinus ostial atresia with persistent left superior vena cava demonstrated on cardiac CT in an infant with a functional single ventricle. *Pediatr Radiol* 2012;42:761-763
61. Agarwal PP, Mahani MG, Lu JC, Dorfman AL. Levoatriocardinal vein and mimics: spectrum of imaging findings. *AJR Am J Roentgenol* 2015;205:W162-W171
62. Takada Y, Narimatsu A, Kohno A, Kawai C, Hara H, Harasawa A, et al. Anomalous left brachiocephalic vein: CT findings. *J Comput Assist Tomogr* 1992;16:893-896
63. Ugas Charcape CF, Alpaca Rodriguez LR, Matos Rojas IA, Lazarte Rantes CI, Valdez Quintana M, Katekaru Tokeshi DA, et al. Characterisation of computed tomography angiography

findings in paediatric patients with heterotaxy. *Pediatr Radiol* 2019;49:1142-1151
64. Montesa C, Karamlou T, Ratnayaka K, Pophal SG, Ryan J, Nigro JJ. Hepatic vein incorporation into the azygos system in heterotaxy and interrupted inferior vena cava. *World J Pediatr Congenit Heart Surg* 2019;10:330-337
65. Nakata T, Fujimoto Y, Hirose K, Osaki M, Tosaka Y, Ide Y, et al. Fontan completion in patients with atrial isomerism and separate hepatic venous drainage. *Eur J Cardiothorac Surg* 2010;37:1264-1270
66. Kim H, Chung JW, Park JH, Yin YH, Park SH, Yoon CJ, et al. CT venography in the diagnosis and treatment of benign thoracic central venous obstruction. *Korean J Radiol* 2003;4:146-152
67. Goo HW. *Chapter 3. CT in pediatric heart disease*. In: Saremi F, Achenbach S, Arbustini E, Narula J, eds. *Revisiting cardiac anatomy: a computed-tomography-based atlas and reference*. Oxford: Wiley-Blackwell, 2011:76-84
68. Truong QA, Yared K, Maurovich-Horvat P, Siegel E, Cubeddu RJ, King ME, et al. Images in cardiovascular medicine. Double-chambered right ventricle and situs inversus with dextrocardia. *Circulation* 2010;121:e229-e232
69. Inoue Y, Igawa O, Iitsuka K. Aneurysm of the right ventricular outflow tract after surgical repair of Tetralogy of Fallot: three-dimensional computed tomography findings. *Europace* 2009;11:130
70. Nakazono T, Jeudy J, White CS. Left and right ventricular diverticula: incidence and imaging findings on 256-slice multidetector computed tomography. *J Thorac Imaging* 2012;27:179-183
71. Ojha V, Chandrashekhara SH, Ganga KP, Saxena A, Gulati G. Congenital left ventricular diverticulum in pentalogy of cantrell: puzzle solved with dual-source CT. *Ann Thorac Surg* 2019;108:e205
72. Nakagawa M, Hara M, Sakurai K, Ohashi K, Asano M, Shibamoto Y. Usefulness of electrocardiography-gated dual-source computed tomography for evaluating morphological features of the ventricles in children with complex congenital heart defects. *Jpn J Radiol* 2011;29:540-546
73. Dydynski PB, Kiper C, Kozik D, Keller BB, Austin E, Holland B. Three-dimensional reconstruction of intracardiac anatomy using CTA and surgical planning for double outlet right ventricle: early experience at a tertiary care congenital heart center. *World J Pediatr Congenit Heart Surg* 2016;7:467-474
74. Yim D, Dragulescu A, Ide H, Seed M, Grosse-Wortmann L, van Arsdell G, et al. Essential modifiers of double outlet right ventricle: revisit with endocardial surface images and 3-dimensional print models. *Circ Cardiovasc Imaging* 2018;11:e006891
75. Goo HW, Park SJ, Yoo SJ. Advanced medical use of three-dimensional imaging in congenital heart disease: augmented reality, mixed reality, virtual reality, and three-dimensional printing. *Korean J Radiol* 2020;21:133-145
76. Goo HW. Myocardial delayed-enhancement CT: initial experience in children and young adults. *Pediatr Radiol* 2017;47:1452-1462
77. Han BK, Hlavacek AM, Kay WA, Pham TDN, Grant K, Garberich RF, et al. Multi-institutional evaluation of the indications and radiation dose of functional cardiovascular computed tomography (CCT) imaging in congenital heart disease. *Int J Cardiovasc Imaging* 2016;32:339-346
78. Goo HW. Serial changes in anatomy and ventricular function on dual-source cardiac computed tomography after the Norwood procedure for hypoplastic left heart syndrome. *Pediatr Radiol* 2017;47:1776-1786
79. Goo HW. Changes in right ventricular volume, volume load, and function measured with cardiac computed tomography over the entire time course of tetralogy of Fallot. *Korean J Radiol* 2019;20:956-966
80. Goo HW. Quantification of initial right ventricular dimensions by computed tomography in infants with congenital heart disease and a hypoplastic right ventricle. *Korean J Radiol* 2020;21:203-209
81. Goo HW. Technical feasibility of semiautomatic three-dimensional threshold-based cardiac computed tomography quantification of left ventricular mass. *Pediatr Radiol* 2019;49:318-326
82. Buss SJ, Schulz F, Mereles D, Hosch W, Galuschky C, Schummers G, et al. Quantitative analysis of left ventricular strain using cardiac computed tomography. *Eur J Radiol* 2014;83:e123-e130
83. Goo HW, Park SH. Pattern analysis of left ventricular remodeling using cardiac computed tomography in children with congenital heart disease: preliminary results. *Korean J Radiol* 2020;21:717-725
84. Malik SB, Kwan D, Shah AB, Hsu JY. The right atrium: gateway to the heart--anatomic and pathologic imaging findings. *Radiographics* 2015;35:14-31
85. Goo HW. Haemodynamic findings on cardiac CT in children with congenital heart disease. *Pediatr Radiol* 2011;41:250-261
86. Saremi F. *Cardiac shunts: ASD, VSD, PDA*. In: Saremi F, ed. *Cardiac CT and MR for adult congenital heart disease*, 1st ed. New York: Springer, 2014:305-345
87. Yasunaga D, Hamon M. MDCT of interatrial septum. *Diagn Interv Imaging* 2015;96:891-899
88. Sun L, Juan YH, Chen J, Zhuang J, Xie J, Li H, et al. Evaluation of unroofed coronary sinus syndrome using cardiovascular CT angiography: an observational study. *AJR Am J Roentgenol* 2018;211:314-320
89. Malik A, Fram D, Mohani A, Fischerkeller M, Yekta A, Mohyuddin Y, et al. Cor triatriatum: a multimodality imaging approach. *Can J Cardiol* 2008;24:e19-e20
90. Thakrar A, Shapiro MD, Jassal DS, Neilan TG, King ME, Abbara S. Cor triatriatum: the utility of cardiovascular imaging. *Can J Cardiol* 2007;23:143-145
91. Sánchez-Brotons JA, López-Pardo FJ, Rodríguez-Puras MJ, López-Haldón JE. Cor triatriatum dexter in adults. *Rev Esp*

https://doi.org/10.3348/kjr.2020.1332

Cardiol 2010;63:998-999
92. Goo HW. Evaluation of the airways in patients with congenital heart disease using multislice CT. *J Korean Pediatr Cardiol Soc* 2004;8:37-43
93. Jhang WK, Park JJ, Seo DM, Goo HW, Gwak M. Perioperative evaluation of airways in patients with arch obstruction and intracardiac defects. *Ann Thorac Surg* 2008;85:1753-1758
94. Etesami M, Ashwath R, Kanne J, Gilkeson RC, Rajiah P. Computed tomography in the evaluation of vascular rings and slings. *Insights Imaging* 2014;5:507-521
95. Lee EY, Zucker EJ, Restrepo R, Daltro P, Boiselle PM. Advanced large airway CT imaging in children: evolution from axial to 4-D assessment. *Pediatr Radiol* 2013;43:285-297
96. Ming Z, Lin Z. Evaluation of tracheal bronchus in Chinese children using multidetector CT. *Pediatr Radiol* 2007;37:1230-1234
97. Yamoto M, Fukumoto K, Sekioka A, Iwazaki T, Sano K, Takahashi T, et al. Non-operative management of congenital tracheal stenosis: criteria by computed tomography. *Pediatr Surg Int* 2019;35:1123-1130
98. Masrani A, McWilliams S, Bhalla S, Woodard PK. Anatomical associations and radiological characteristics of Scimitar syndrome on CT and MR. *J Cardiovasc Comput Tomogr* 2018;12:286-289
99. Goo HW, Kim YH, Ko JK, Park IS, Yoon CH. Horseshoe lung: useful angiographic and bronchographic images using multidetector-row spiral CT in two infants. *Pediatr Radiol* 2002;32:529-532
100. Long FR, Castile RG. Technique and clinical applications of full-inflation and end-exhalation controlled-ventilation chest CT in infants and young children. *Pediatr Radiol* 2001;31:413-422
101. Goo HW, Kim HJ. Detection of air trapping on inspiratory and expiratory phase images obtained by 0.3-second cine CT in the lungs of free-breathing young children. *AJR Am J Roentgenol* 2006;187:1019-1023
102. Chen SJ, Li YW, Wang JK, Wu MH, Chiu IS, Chang CI, et al. Usefulness of electron beam computed tomography in children with heterotaxy syndrome. *Am J Cardiol* 1998;81:188-194
103. Wolla CD, Hlavacek AM, Schoepf UJ, Bucher AM, Chowdhury S. Cardiovascular manifestations of heterotaxy and related situs abnormalities assessed with CT angiography. *J Cardiovasc Comput Tomogr* 2013;7:408-416
104. Makhija Z, Marwah A, Mishra S, Kumar J, Goel A, Sharma R. Biventricular repair in heterotaxy patients. *World J Pediatr Congenit Heart Surg* 2015;6:195-202
105. Chen BB, Chen SJ, Wu MH, Li YW, Lue HC. EBCT-McGoon ratio a reliable and useful method to predict pulmonary blood flow non-invasively. *Chinese J Radiol* 2007;32:1-8
106. Park EA, Lee W, Chung SY, Yin YH, Chung JW, Park JH. Optimal scan timing and intravenous route for contrast-enhanced computed tomography in patients after Fontan operation. *J Comput Assist Tomogr* 2010;34:75-81
107. Egbe AC, Reddy YNV, Khan AR, Al-Otaibi M, Akintoye E, Obokata M, et al. Venous congestion and pulmonary vascular function in Fontan circulation: implications for prognosis and treatment. *Int J Cardiol* 2018;271:312-316
108. Lluri G, Levi DS, Aboulhosn J. Systemic to pulmonary venous collaterals in adults with single ventricle physiology after cavopulmonary palliation. *Int J Cardiol* 2015;189:159-163
109. Litmanovich DE, Kirsch J. Computed tomography of cardiac valves: review. *Radiol Clin North Am* 2019;57:141-164
110. Faure ME, Swart LE, Dijkshoorn ML, Bekkers JA, van Straten M, Nieman K, et al. Advanced CT acquisition protocol with a third-generation dual-source CT scanner and iterative reconstruction technique for comprehensive prosthetic heart valve assessment. *Eur Radiol* 2018;28:2159-2168
111. Bang JH, Park JJ, Goo HW. Evaluation of commissural malalignment of aortic-pulmonary sinus using cardiac CT for arterial switch operation: comparison with transthoracic echocardiography. *Pediatr Radiol* 2017;47:556-564
112. Goo HW, Park SH. Computed tomography-based ventricular volumes and morphometric parameters for deciding the treatment strategy in children with a hypoplastic left ventricle: preliminary results. *Korean J Radiol* 2018;19:1042-1052
113. Goo HW. Volumetric severity assessment of Ebstein anomaly using three-dimensional cardiac CT: a feasibility study. *Cardiovasc Imaging Asia* 2019;3:61-67
114. Tomasian A, Malik S, Shamsa K, Krishnam MS. Congenital heart diseases: post-operative appearance on multi-detector CT-a pictorial essay. *Eur Radiol* 2009;19:2941-2949
115. Beerbaum P, Valverde I, Greil GF, Babu-Narayan SV. *Chapter 17. Baffles and conduits*. In: Fogel MA, ed. *Principles and practice of cardiac magnetic resonance in congenital heart disease*, 1st ed. New Jersey: Wiley-Blackwell, 2010:316-344
116. Eichhorn JG, Jourdan C, Hill SL, Raman SV, Cheatham JP, Long FR. CT of pediatric vascular stents used to treat congenital heart disease. *AJR Am J Roentgenol* 2008;190:1241-1246
117. Yoo SJ, Saito M, Hussein N, Golding F, Goo HW, Lee W, et al. Systematic approach to malalignment type ventricular septal defects. *J Am Heart Assoc* 2020;9:e018275

 https://doi.org/10.3348/kjr.2020.1332